Journal of Materials Chemistry C

PAPER

View Article Online
View Journal | View Issue

Check for updates

Cite this: J. Mater. Chem. C, 2019, 7, 10379

Effect of structural engineering of π-spacers on anti-aggregation of D–A–π–A dyes†

Tao Hua,[a] Keyi Zhang,[a] Zu-Sheng Huang,[b] Lingyun Wang,[a] Hao Tang,[a] Herbert Meier*[ac] and Derong Cao*[a]

Received 8th June 2019,
Accepted 26th July 2019

DOI: 10.1039/c9tc03066b

rsc.li/materials-c

In this paper, the encapsulated insulated molecular wire (EIMW) and 2′,7′-bis(hexyloxy)spiro[cyclopenta-[2,1-*b*:3,4-*b*′]dithiophene-4,9′-fluorene] (SPDF) were specifically designed as efficient anti-aggregation π-bridges for two novel D–A–π–A metal-free sensitizers (**IBT1 and IBT2**). Compared with the reference dye **IBT3** with 3,3′-dihexyl-2,2′-bithiophene (DHBT) as an anti-aggregation π-bridge, both the dyes **IBT1** with EIMW and **IBT2** with SPDF as π-bridges can suppress intermolecular aggregation more efficiently. The π-bridge of SPDF shows the strongest anti-aggregation ability due to the rigid 'T' configuration among these dyes. Meanwhile, the π-bridge of EIMW shows better anti-aggregation ability than DHBT because of the larger steric hindrance of the former. Finally, when the dyes **IBT1** and **IBT2** are co-sensitized with **IBT3,** respectively, the new devices exhibit high efficiencies of 7.85% and 7.64%, respectively, which are comparable to that of **N719** (7.85%). The results demonstrate that the dyes with EIMW and SPDF as anti-aggregation π-bridges are promising candidates for efficient DSSCs and dye aggregation can be effectively inhibited by structural engineering of the π-spacer.

Published on 26 July 2019. Downloaded on 1/29/2026 9:17:27 PM.

1. Introduction

Dye-sensitized solar cells (DSSCs) have attracted increasing interest over the last few decades, owing to their unique merits in terms of low-cost production, easy fabrication and good stability.[1–8] DSSCs have been developed to achieve high power conversion efficiency since the work by O'Regan and Grätzel in 1991.[9] The exploration of new-style photosensitizers with broad absorption spectra to achieve high power conversation efficiency (PCE) is a crucial mission for the development of energy technologies. Metal complex dyes and metal-free dyes have been developing rapidly, which significantly improve the performance of the devices,[10–12] especially for metal-free sensitizers, due to the advantages of accessible raw materials, their environmentally friendly nature and highly adjustable structure.[13,14] In recent years, extensive research has been directed toward the design of novel metal-free sensitizers that achieve high efficiencies.[15–19] It is worth noting that a new record efficiency of 14.5% was reported in 2015 by using a cobalt-based liquid electrolyte.[20]

In general, donor (D)–π spacer (π)–acceptor (A) type functional dyes have been extensively used in DSSCs, owing to the strong intramolecular charge transfer (ICT) effect, the electron transfer from donor to acceptor flowing through the π-bridge smoothly.[21–25] Afterwards, a new donor–auxiliary acceptor–π spacer–acceptor (D–A–π–A) configuration was developed, which incorporates an electron withdrawing auxiliary acceptor such as benzothiadiazole (BTD),[26,27] benzotriazole (BTZ),[28,29] quinoxaline,[30–32] diketopyrrolopyrrole (DPP),[33,34] isoindigo[35] and 4,4-difluoro-4-bora-3*a*,4*a*-diaza-*s*-indacene (Bodipy).[36,37] Because the new architecture (D–A–π–A) can not only narrow the band gap but also broaden the light absorption in the visible and near infrared regions, these dyes are considered as candidate sensitizers for achieving more efficient DSSCs.[38–41] Cyclopenta[2,1-*b*:3,4-*b*′]dithiophene (CPDT) is extensively used as a π-bridge in the D–A–π–A architecture,[42–45] because of its excellent light-harvesting performance. However, the characteristic rigid planar conformation of this architecture might form a rigid rod shape that facilitates dye aggregation after these dyes are adsorbed onto the surface of TiO_2. All of the reported CPDT sensitizers adopt a conventional alkyl chain as an anti-aggregation group to inhibit dye aggregation, and unfortunately the aggregation behavior still exists,[46–48] which limits further improvement of the device performance.

Dye aggregation is adverse for DSSCs because it lowers the photoelectric performance.[49] Therefore, so far, there have been enormous efforts in designing anti-aggregation dyes.[50–53]

[a] State key Laboratory of Luminescent Materials and Devices, School of Chemistry and Chemical Engineering, South China University of Technology, Guangzhou 510641, China. E-mail: drcao@scut.edu.cn
[b] School of Pharmaceutical Sciences, Wenzhou Medical University, Wenzhou 325035, China
[c] Institute of Organic Chemistry, University of Mainz, Mainz 55099, Germany. E-mail: hmeier@uni-mainz.de

† Electronic supplementary information (ESI) available: Complete experimental details, ^{1}H NMR and ^{13}C NMR spectra of the new compounds, spectroscopic data. See DOI: 10.1039/c9tc03066b

Published on 26 July 2019. Downloaded on 1/29/2026 9:17:27 PM.

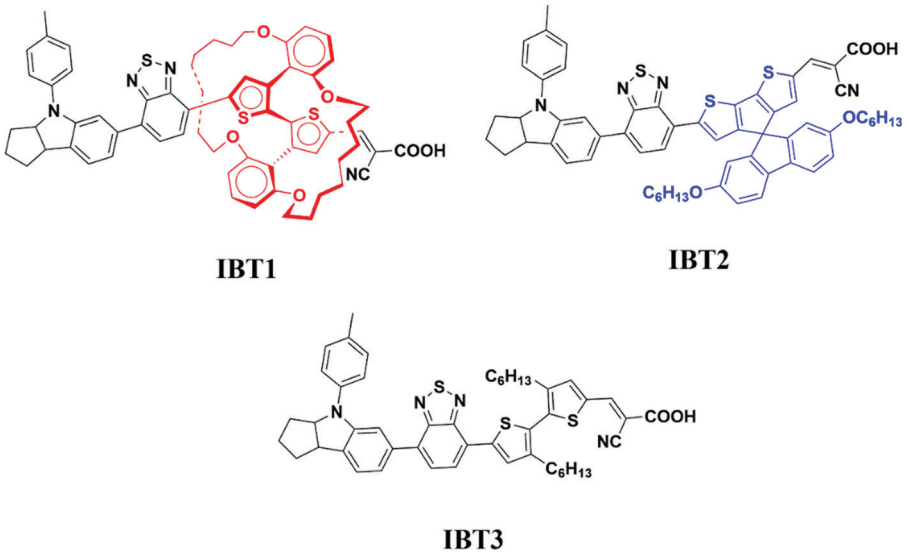

Fig. 1 Chemical structures of indoline based D–A–π–A sensitizers **IBT1–3**.

In our previous work, we have designed and synthesized a series of novel phenothiazine sensitizers **PH1–3**, where the encapsulated insulated molecular wire (EIMW) unit as an auxiliary donor was introduced to the phenothiazine-based organic dyes.[54] The result indicates that the EIMW unit as an auxiliary donor can inhibit dye aggregation dramatically and result in a much higher photovoltage. However, there is still a small amount of aggregation in the dyes. When a coplanar aromatic polycycle was introduced, the new dye aggregation was aggravated significantly.

In this work, we attempted to suppress dye aggregation by π-spacer structural engineering with a 'T' configuration and large steric hindrance. Firstly, we introduced the EIMW unit to the D–A–π–A dye **IBT1** as an anti-aggregation π-spacer with large steric hindrance (Fig. 1). Secondly, we introduced the 2′,7′-bis(hexyloxy)spiro[cyclopenta[2,1-*b*:3,4-*b*′]dithiophene-4,9′-fluorene] (SPDF) unit with a 'T' configuration to suppress dye aggregation in the dye **IBT2**. To the best of our knowledge, SPDF is applied as an anti-aggregation π-spacer for the first time. In addition, 3,3′-dihexyl-2,2′-bithiophene was introduced to achieve **IBT3** as the reference dye because it is well known that alkyl chains show good anti-aggregation effects.[55–58]

2. Experimental

2.1 Materials and reagents

The raw materials were purchased from Aladdin, J&K, Energy Chemical and Adamas and were of analytical grade. Toluene, THF, 1,2-dichloroethane and 1,4-dioxane were distilled over sodium under an argon atmosphere. DMF was extra dried and stored in EnergySeal with molecular sieves. Other solvents and reagents were of analytical grade and used without further purification. The reactions were monitored by thin-layer chromatography (TLC) until the reaction was completed. Chromatographic separations were carried out on silica gel (200–300 mesh).

2.2 Instruments and characterization

Characterization ^{1}H and ^{13}C NMR spectra were recorded on a Bruker advance III 400 MHz spectrometer in $CDCl_3$ and THF-d_8 with tetramethylsilane as the internal standard. High-resolution mass spectrometry (HRMS) spectra were recorded on an Agilent Technologies 1290 Infinity mass spectrophotometer. Melting point was measured on an SGW X-4B microscopic melting point apparatus. The absorption spectra of dyes in solution were measured on a Shimadzu UV-2450 spectrophotometer. The absorption spectra of dyes adsorbed on the surface of TiO_2 were recorded on a UV-3010 spectrophotometer. The PL spectra were recorded on a Fluorolog III photoluminescence spectrometer. The cyclic voltammetry (CV) data were measured with a CHI 660d electrochemical workstation (Chenhua Co. Ltd, Shanghai, China), using a three electrode cell at a scan rate of 50 mV s^{-1}. The dye loaded TiO_2 film was used as a working electrode, a Pt wire as auxiliary electrode, and Ag/AgCl (0.01 M) as reference electrode. The supporting electrolyte was 0.1 M tetrabutylammonium hexafluorophosphate (n-Bu_4NPF_6) in CH_3CN solution. A ferrocenium/ferrocene (Fc/Fc^+) redox couple was employed to act as an internal potential reference. The incident monochromatic photon-to-current conversion efficiency (IPCE) spectra were measured on a Spectral products DK240 monochromator in the region from 400 to 800 nm. The current–voltage characteristics were measured on a Keithley 2400 source meter under simulated AM 1.5G (100 mW cm^{-2}) illumination with a standard solar light simulator with a mask. The electrochemical impedance spectra (EIS) were recorded on a Zahner Zennium electrochemical workstation under dark conditions.

2.3 Fabrication of dye-sensitized solar cells

The manufacturing processes of these cells were carried out according to the previous procedures.[59–61] Fluorine-doped tin oxide (FTO) glass was washed with detergent, water, ethanol and acetone in an ultrasonic bath to wipe off the impurity.

 This journal is © The Royal Society of Chemistry 2019

Published on 26 July 2019. Downloaded on 1/29/2026 9:17:27 PM.

The thickness of the TiO_2 photoanode films was controlled to about 16 μm (12 μm thick transparent layer and 4 μm thick scattering layer). The films were immersed into a 3.0×10^{-4} M solution of the dyes for 24 h (the solution is a mixture solvent of $CHCl_3$ and ethanol (volume ratio of 1 : 1)) at 25 °C. The composition of the electrolyte is 0.6 M 1-metyl-3-propylimidazoliumiodide (PMII), 0.05 M LiI, 0.10 M guanidiniumthiocyanate, 0.03 M I_2 and 0.5 M *tert*-butylpridine in acetonitrile/valeronitrile (85/15). For the co-adsorption, chenodeoxycholic acid (CDCA) was added into the dye solution at a concentration of 1 mM. The dye-loaded TiO_2/FTO glass films were assembled into a sandwiched type configuration together with a Pt/FTO counter electrode. The active area of the dye coated TiO_2 film was 0.16 cm^2. For the co-sensitization experiment, the photoanodes was first immersed into a 0.3 mM solution of dye **IBT1** (or **IBT2**) in $CHCl_3/CH_3CH_2OH$ (v/v, 1/1) for 24 h, rinsed with ethanol, and then immersed into a 0.3 mM solution of dye **IBT3** in $CHCl_3/CH_3CH_2OH$ (v/v, 1/1) for 3 h.

3. Results and discussion

3.1 Synthesis

The synthetic procedures of **IBT1–3** are depicted in Scheme 1. Compound **1**,[62] 5′-bromo-3,3′-dihexyl-[2,2′-bithiophene]-5-carbaldehyde (**7**),[63] 4-(4,4,5,5-tetramethyl-1,3,2-dioxaborolan-2-yl)-7-(4-(*p*-tolyl)-1,2,3,3*a*,4,8*b*-hexahydrocyclopenta[*b*]indol-6-yl)benzo[*c*][1,2,5]thiadiazole (**8**)[64] and 2′,7′-bis(hexyloxy)spiro[cyclopenta[2,1-*b*:3,4-*b*′]dithiophene-4,9′-fluorene] (SPDF) (**4**)[65] were synthesized according to the references. Intermediates **3**, **6** and **9** were synthesized *via* the Suzuki coupling reaction. Intermediates **5** and **8** were synthesized according to the Vilsmeier–Haack reaction and then through bromination with *N*-bromosuccinimide (NBS). The target products **IBT1**, **IBT2** and **IBT3** were obtained from **3**, **6** and **9** *via* the Knoevenagel condensation reaction. All of the new compounds were certified by ^{1}H NMR, ^{13}C NMR and HRMS or MALDI-TOF-MS.

3.2 Photophysical properties

The UV-Vis absorption spectra of the three dyes **IBT1**, **IBT2** and **IBT3** were measured in CH_2Cl_2 solution (Fig. 2) and relevant characteristic data are tabulated in Table 1. Generally, the three dyes show two obvious broad absorption bands in the range of 300–750 nm. The high-energy bands located at 300–380 nm are generated by a local aromatic π–π* electronic transition of the chromophores. The low-energy bands located at 380–750 nm are produced by intramolecular charge transfer (ICT) from the indoline donor to the electron acceptor of cyanoacetic acid. The maximum absorption wavelengths of **IBT1**, **IBT2** and **IBT3** are 544, 564 and 513 nm, respectively. Compared with **IBT3**, **IBT1** and **IBT2** display a distinct red shift of 31 nm and 51 nm in the ICT absorption band, respectively; this phenomenon may be attributed to the better and better planarity obtained when EIMW and SPDF are introduced in turn. Besides, additional bands are found in the range of 400–500 nm for **IBT1** and **IBT2.** The origin of these bands has been researched in a previously reported reference.[66] Special mention should be made that dye **IBT3** achieved a higher absorption in the range of 300–500 nm than **IBT1** and **IBT2**, and this phenomenon suggests that **IBT3**

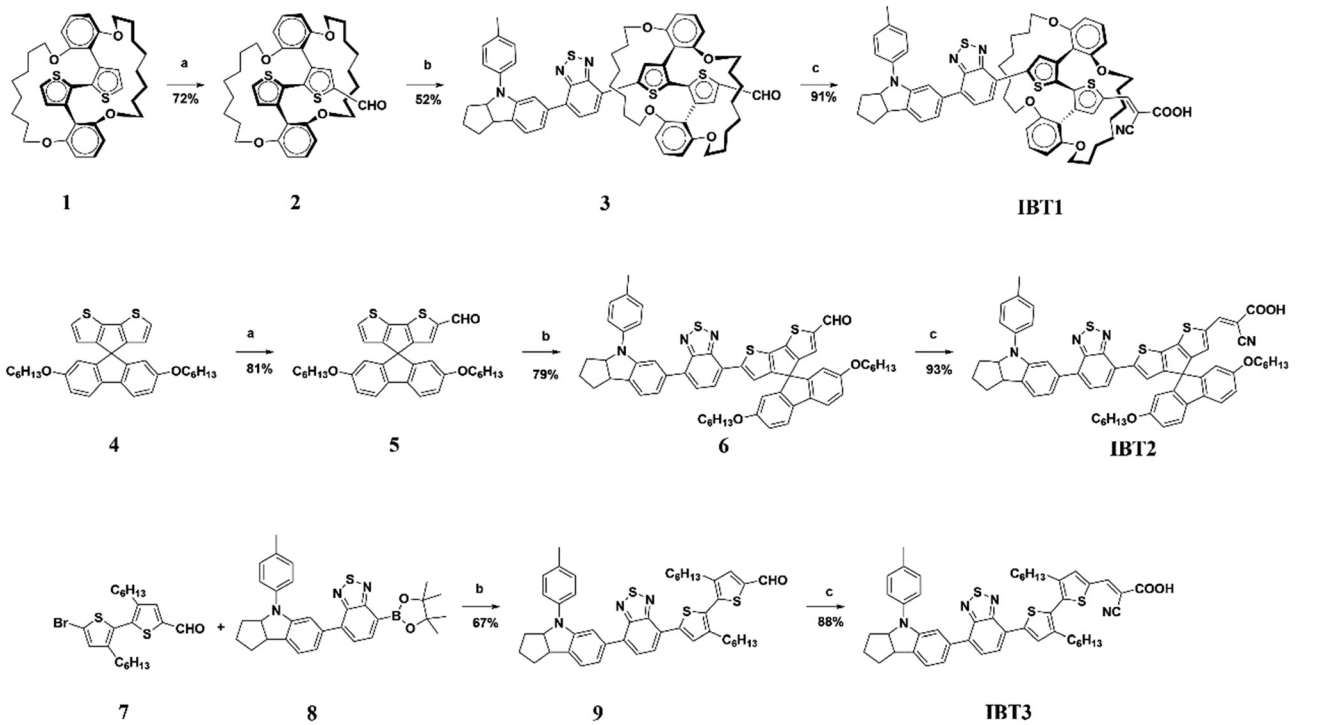

Scheme 1 Synthetic routes of the dyes **IBT1–3**. (a) $POCl_3$, DMF, and 1,2-dibromoethane, at 80 °C; (b) $Pd(PPh_3)_4$, Na_2CO_3, ethanol, H_2O, and toluene, at 100 °C; (c) piperidine, cyanoacetic acid, and $CHCl_3$, at 75 °C.

Published on 26 July 2019. Downloaded on 1/29/2026 9:17:27 PM.

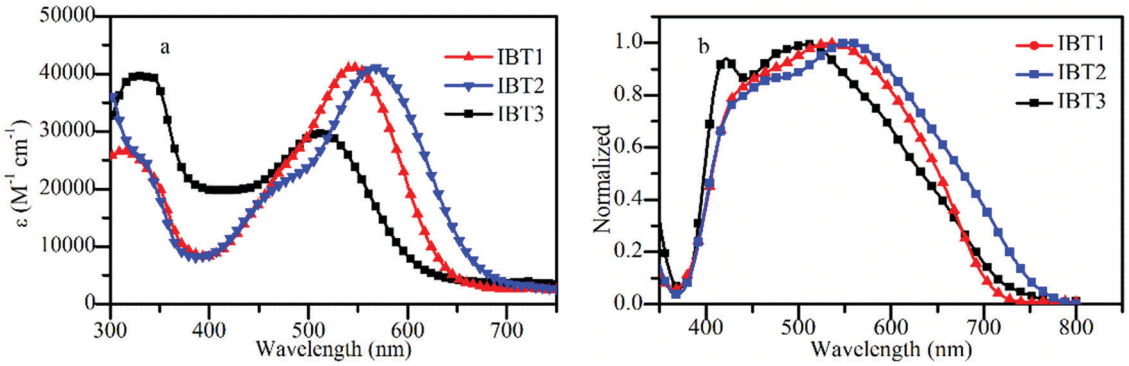

Fig. 2 The UV-Vis absorption spectra of the three dyes in CH_2Cl_2 solution (a) and the absorption spectra on 12 μm TiO_2 films (b).

Table 1 Optical and electrochemical data of the dyes **IBT1–3**

Dye	λ_{max}[a] (nm)	ε[a] (10^4 M^{-1} cm^{-1})	λ_{max}[b] (nm)	HOMO[c] (V)	E_{0-0}[d] (eV)	LUMO[e] (V)
IBT1	544	4.11	532	0.87	2.13	−1.26
IBT2	564	4.10	554	0.85	1.96	−1.11
IBT3	513	2.97	505	0.85	2.18	−1.33

[a] Maximum absorption peak (λ_{max}) and molar extinction coefficient (ε) of the dyes were measured in CH_2Cl_2 solution. [b] λ_{max} of the dyes was measured on 12 μm TiO_2 films. [c] Oxidation potential was measured in CH_3CN containing 0.1 M $(n\text{-}C_4H_9)_4NPF_6$ with a scan rate of 50 mV s^{-1}, referenced against Fc/Fc^+. [d] E_{0-0} was estimated from the normalized fluorescence and absorption curves by $1240/\lambda$ in CH_2Cl_2 solution. [e] The LUMO was calculated according to LUMO = HOMO − E_{0-0}.

might be a co-sensitizer for dyes **IBT1** and **IBT2** to make up the absorption valley in this region.

In addition, the three dyes achieve a high molar extinction coefficient, especially dyes **IBT1** and **IBT2**. For dye **IBT3**, two alkyl chains were introduced to suppress dye aggregation and increase solubility, but a smaller molar extinction coefficient (2.97×10^4 M^{-1} cm^{-1}) was obtained due to the interrupted conjugation resulting from two alkyl chains, which can be verified later by the DFT calculation. Compared to dye **IBT3**, **IBT1** showed a higher molar extinction coefficient (4.11×10^4 M^{-1} cm^{-1}) after EIMW was introduced. **IBT2** with a novel π bridge SPDF shows the same high molar extinction coefficient (4.10×10^4 M^{-1} cm^{-1}) as **IBT1**. These results suggest that both **IBT1** and **IBT2** possess stronger light-harvesting capability.[67]

The absorption spectra of **IBT1–3** on 16 μm thick TiO_2 films are shown in Fig. 2b and the corresponding data are listed in Table 1. The absorption spectra of these dyes are broadened in comparison with those in solution, which is beneficial for improving the light-harvesting ability. In contrast with those in solution, the maximum absorption peak (λ_{max}) of **IBT1**, **IBT2** and **IBT3** exhibits a blue shift of 12, 10 and 8 nm, respectively. This phenomenon may be due to a deprotonation effect and dye aggregation. It is surprising that **IBT2** shows the widest absorption spectrum, which demonstrates that SPDF might be a potential light-harvesting segment in the field of DSSCs.

3.3 Electrochemical properties

The thermodynamic possibility of electron injection, dye regeneration and electrochemical properties of the three dye sensitized films were determined by cyclic voltammetry in MeCN solution with 0.1 M tetrabutyl-ammonium hexafluorophosphate as the supporting electrolyte. The first oxidation potential corresponds to the highest occupied molecular orbital (HOMO) level. The cyclic voltammetry curves and schematic diagram of energy levels of all **IBT** sensitizers are shown in Fig. 3, and the corresponding electrochemical data are listed in Table 1. The potential was externally calibrated by the ferrocenium/ferrocene (Fc/Fc^+) couple and then converted

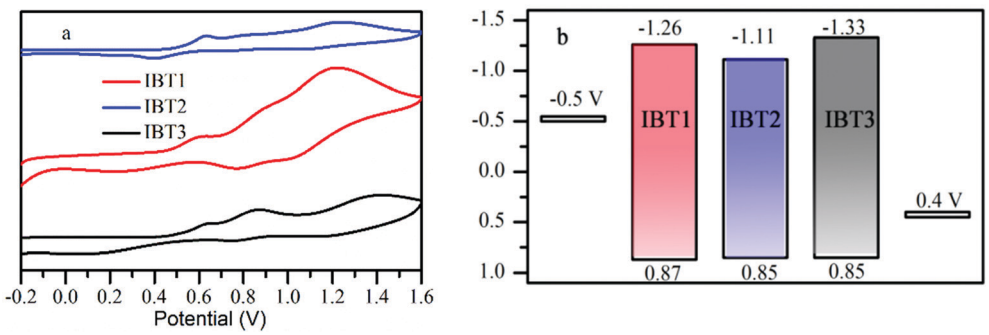

Fig. 3 (a) Cyclic voltammograms of the three dye sensitized films in acetonitrile containing 0.1 M $(n\text{-}C_4H_9)_4NPF_6$ as the supporting electrolyte and (b) the HOMO and LUMO of the three dyes.

 This journal is © The Royal Society of Chemistry 2019

Published on 26 July 2019. Downloaded on 1/29/2026 9:17:27 PM.

to NHE by addition of 0.63 V. The HOMO levels of the dyes **IBT1**, **IBT2** and **IBT3** are 0.87 V, 0.85 V and 0.85 V, respectively. These nearly identical values are mainly ascribed to the same donor of the dyes, because the HOMO level depends on the donor segment.[68] These values are more positive than the I^-/I_3^- redox potential value (0.4 V *vs.* NHE), which indicates that the oxidized dyes can be efficiently regenerated by the electrolyte. Estimated from the intersection of the normalized absorption and emission spectra, E_{0-0} values of **IBT1**, **IBT2** and **IBT3** are 2.13, 1.96 and 2.18 eV, respectively. The LUMO levels of dyes **IBT1**, **IBT2** and **IBT3** calculated from HOMO–E_{0-0} are −1.26, −1.11 and −1.33 V, respectively. The values are more negative than the conduction band (CB) level of TiO_2 (−0.5 V *vs.* NHE), indicating that an efficient electron injection process from the excited dye into the conduction band of TiO_2 can occur for the three dyes.[69]

3.4 Theoretical calculations

To investigate the electron-density distributions of the three dyes, we used the hybrid B3LYP functional and the 6-31G(d) basis set to optimize the ground-state geometries of the sensitizers in the gas phase by density functional theory (DFT) simulation with the Gaussian 09 package. The optimized molecular configurations and distributions of the HOMO and LUMO orbitals of the three dyes are shown in Table 2. The optimized molecular configuration of **IBT3** shows a lengthy rodlike structure, which tends to aggravate dye aggregation, therefore, leading to self-quenching and inefficient electron injection into the TiO_2. It is worth noting that these deleterious processes can be avoided or suppressed in **IBT1** and **IBT2**, because the two dyes possess bulky structural features that impede aggregation.[70] For **IBT1**, the rod-shaped configuration is surrounded by a circle alkyl chain, so the dye–dye interaction on the surface of TiO_2 is controlled. A peculiar cross-shaped rigid structure is found in **IBT2**, which reduces the tendency to form aggregations due to the inhibition of intermolecular interactions.[71] These results are consistent with the conclusions of the anti-aggregation ability.

For the dyes **IBT1** and **IBT2**, the HOMO orbitals are delocalized over the whole D–A–π portion, but mainly delocalized over the D–A portion for **IBT3**. The difference is caused by the fact that the two alkyl chains between the two thiophene units break the planarity of the skeleton. This result is confirmed by the following dihedral angle calculation. The LUMO orbitals of the three dyes are distributed along the A–π–A section. Besides, the HOMO and LUMO orbitals of **IBT1–3** have obvious overlap on the additional acceptor BTD group, which can promote electron transfer from the indoline donor to the cyanoacetic acid acceptor.

The dihedral angles of each part were achieved through the optimized ground-state geometries of these sensitizers. The dihedral angles between the extra-acceptor and the π-spacer of **IBT1**, **IBT2** and **IBT3** are 0.9°, 1.5° and 1.5°, respectively. This result shows no obvious effect on the planarity of the D–A part when introducing different π-spacers into the skeleton of the three dyes. The dihedral angles between the bithiophene units are 0.6°, 0° and 49.8°, respectively. It can be found that **IBT1** and **IBT2** possess excellent planarity of the π-spacer, which is beneficial to charge transfer from the donor to the acceptor. On the contrary, dye **IBT3** shows the biggest twist angle between the two thiophene units, leading to a blue-shifted maximum absorption wavelength and lower molar extinction coefficient. The twist angles between π-spacer and acceptor of **IBT1**, **IBT2** and **IBT3** are 0.2°, 0.1° and 3.0°, respectively. The superior planarity of the π–A part is beneficial to electron injection into the conduction band of TiO_2.

3.5 Photovoltaic performance of the DSSCs

The cells based on **IBT1–3** were fabricated with iodine electrolyte and the photovoltaic properties of the dyes were determined (Fig. 4). The relevant parameters are listed in Table 3. The photocurrent–voltage (*J–V*) measurements are exhibited in Fig. 4a. The devices based on **IBT1**, **IBT2** and **IBT3** show a PCE of 6.92%, 6.67% and 7.21%, respectively. The dye **IBT3** achieves the highest efficiency, producing a short-circuit photocurrent (J_{sc})

Table 2 Optimized structures and electron distributions in the HOMO and LUMO levels of the dyes **IBT1–3**

Dye	Optimized structure	HOMO	LUMO
IBT1	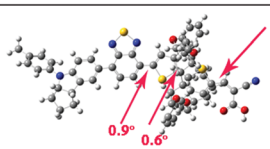	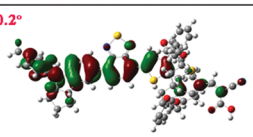	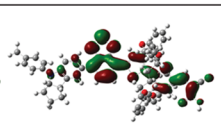
IBT2	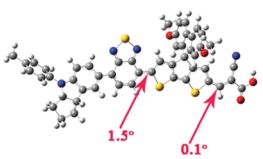	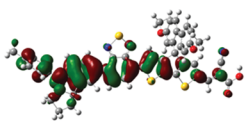	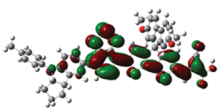
IBT3	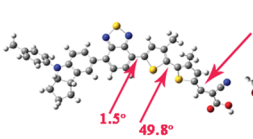	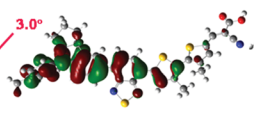	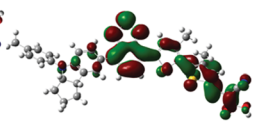

Published on 26 July 2019. Downloaded on 1/29/2026 9:17:27 PM.

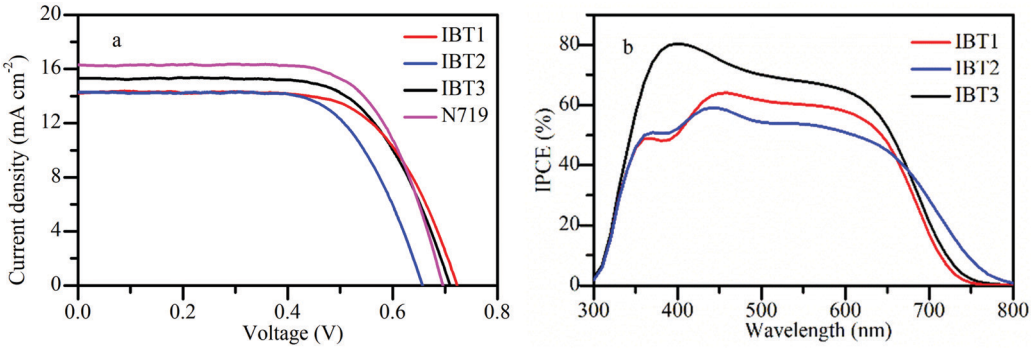

Fig. 4 *J–V* curves (a) and IPCE spectra (b) of DSSCs based on **IBT1–3**.

Table 3 Photovoltaic parameters of the devices sensitized with **IBT1–3**

Dye	J_{sc} (mA cm^{-2})	V_{oc} (mV)	FF (%)	PCE (%)	Dye loading amount ($\times 10^{-7}$ mol cm^{-2})	
IBT1[a]	14.30	722	0.67	6.92	1.09	
IBT2[a]	14.55	665	0.69	6.67	1.66	
IBT3[a]	15.17	689	0.69	7.21	2.50	
IBT1 + **CDCA**[b]	14.05	728	0.68	6.96	—	
IBT2 + **CDCA**[b]	14.01	669	0.69	6.47	—	
IBT3 + **CDCA**[b]	15.43	721	0.68	7.56	—	
IBT1 + **IBT3**[c]	15.83	729	0.68	7.85	1.04 (**IBT1**)	0.648 (**IBT3**)
IBT2 + **IBT3**[c]	16.21	693	0.68	7.64	1.49 (**IBT2**)	0.948 (**IBT3**)
N719[a]	16.53	698	0.68	7.85		

[a] The photoanodes were immersed in a 0.3 mM solution of the three dyes in $CHCl_3/CH_3CH_2OH$ (v/v, 1/1) for 24 h. [b] CDCA was added into the dye solution at a concentration of 1 mM. [c] The photoanodes were first immersed in a 0.3 mM solution of **IBT1** (or **IBT2**) in $CHCl_3/CH_3CH_2OH$ (v/v, 1/1) for 24 h, rinsed with ethanol, and then immersed into a 0.3 mM solution of **IBT3** in $CHCl_3/CH_3CH_2OH$ (v/v, 1/1) for 3 h.

of 15.17 mA cm^{-2}, an open-circuit photovoltage (V_{oc}) of 689 mV and a fill factor (FF) of 0.69. As listed in Table 3, the loading amounts of dyes **IBT1**, **IBT2** and **IBT3** are 1.09×10^{-7} mol cm^{-2}, 1.66×10^{-7} mol cm^{-2} and 2.50×10^{-7} mol cm^{-2}, respectively. Compared with **IBT3**, **IBT1** and **IBT2** show a relatively lower efficiency, which might be due to the lower loading amount on the surface of TiO_2.[69] The device based on **IBT1** presents the highest V_{oc} because EIMW is introduced as a π-spacer. EIMW has a rotaxane-like configuration, the circle chain plays a role as a compact layer on the surface of TiO_2. The compact layer produces an efficient shielding effect to retard the I_3^- ion from approaching the TiO_2 surface and reduces the charge recombination rate. Therefore, the DSSC based on **IBT1** achieved the highest V_{oc}.[54,72] The reason that the alkyl chain can inhibit charge recombination is similar to that of EIMW,[43,68] but the circle chain weakens charge recombination more effectively than the linear alkyl chain. Consequently, the V_{oc} of the device based on **IBT3** is lower than **IBT1**. However, for **IBT2** with SPDF as π-spacer, a large steric hindrance is obtained, the gap between the two molecular frames is oversized, the charge recombination is easier, and so the V_{oc} of the DSSC based on **IBT2** drops significantly.

In order to investigate the relationship between the structure and performance, the theoretical efficiencies of the three dyes are calculated based on the same adsorption amount as the dye **IBT2** (1.66×10^{-7} mol cm^{-2}). The calculated efficiencies of the dyes **IBT1**, **IBT2** and **IBT3** are 10.50%, 6.67% and 4.79%, respectively, if the same adsorption amount is 1.66×10^{-7} mol cm^{-2}. This result manifests that the anti-aggregation characteristic of the two featured π-spacers (EIMW and SPDF) is favorable for harvesting the sunlight and obtaining excellent photoelectric performance.

In order to explain the tendency of J_{sc} reasonably, the incident photo-to-current conversion efficiency (IPCE) spectra were measured and the results are shown in Fig. 4b. In the range of 300–670 nm, the plateaus of the IPCE spectrum become higher and higher in the order of **IBT2** < **IBT1** < **IBT3**, so these behaviors are consistent with the variation in J_{sc}. Meanwhile, the device based on dye **IBT2** shows the widest IPCE response. This phenomenon is consistent with the previous UV-Vis absorption spectra (Fig. 2). For dye **IBT2**, a lower plateau results from the decreased loading amount, but it exhibits a wider light-harvesting region, along with no distinct valley over the whole visible wavelength. This phenomenon indicates that the SPDF as a π-bridge might have great potential in the photoelectronic field.

3.6 Anti-aggregation ability

Dye aggregation is a negative factor in DSSCs. Unfortunately, it is a common phenomenon, especially for planar dyes. We have reported an organic dye **PH2** (Fig. S17, ESI†) with EIMW as an auxiliary donor to suppress dye aggregation in DSSCs considering that EIMW is a big ring with large steric hindrance. The results show that EIMW is a good auxiliary donor to suppress dye aggregation. In this study, we focused on the effect of structural engineering of the π-spacer with EIMW and DHBT to suppress dye aggregation in DSSCs. The dye **IBT3** with 3,3′-dihexyl-2,2′-bithiophene as π-bridge was chosen as the reference dye because two alkyl chains in the π-bridge show a good anti-aggregation effect.

It is well known that chenodexycholic acid (CDCA) is usually used as a co-adsorbent to inhibit dye aggregation. But for an anti-aggregation dye, the J_{sc} would decrease because of competitive adsorption, which would not improve the photoelectric performance after addition of CDCA.[73] In this work, an appropriate amount (1 mM) of CDCA was added to verify whether the two π-bridges can suppress dye aggregation. The *J–V* characteristics of the DSSCs are exhibited in Fig. 5 and relevant photovoltaic data are listed in Table 3. When CDCA was added, the efficiency of the device based on **IBT3** was improved from 7.21% to 7.53%, which means that there is still aggregation even though

 This journal is © The Royal Society of Chemistry 2019

Published on 26 July 2019. Downloaded on 1/29/2026 9:17:27 PM.

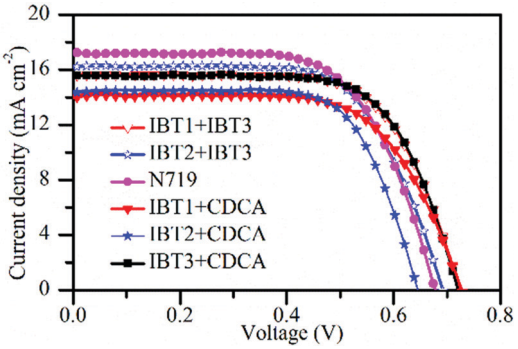

Fig. 5 *J–V* characteristics of DSSCs based on six devices.

the two alkyl chains in the π-bridge act as good anti-aggregation groups. However, the J_{sc} values of the two devices based on **IBT1** and **IBT2** show a slight decrease because of competitive adsorption. The efficiency shows only a minor variation for **IBT1**, which demonstrates that EIMW exhibits better anti-aggregation ability than alkyl chains. The higher anti-aggregation of EIMW might be rationalized by its larger steric hindrance. More interestingly, the PCE of the cell based on **IBT2** slightly declined, which demonstrates that SPDF exhibits the strongest anti-aggregation ability due to the rigid 'T' configuration among these dyes. SPDF has a peculiar rigid 'T' structure with two perpendicularly oriented molecular halves. The 3-dimensional structure can inhibit intermolecular interactions efficaciously. However, EIMW and the linear alkyl chain can also inhibit dye aggregation, but these are stretchable architectures; when the dyes are adsorbed on the surface of TiO_2, the alkyl chain of the two π-spacers can move freely within a certain range, so the π–π stacking is eliminated incompletely. Therefore, the flexible structure leads to a weaker anti-aggregation ability than the rigid structure. In comparison with the dye **PH1** with EIMW as an auxiliary donor, **IBT1** shows more effective anti-aggregation ability when EIMW is introduced as a π-bridge, which suggests that the anti-aggregation effect of the EIMW unit as a π-bridge is more efficacious than as an auxiliary donor.

3.7 Co-sensitization

In order to reduce the deficiencies that result from the low loading amount and the limit of the light-harvesting region, co-sensitization tactics were applied to improve the photovoltaic performance. As mentioned above, **IBT1** and **IBT2** show an obvious absorption valley in the range of 300–500 nm, but on the contrary, **IBT3** shows a notable absorption peak in this region (Fig. S18 and S19, ESI†). The absorption spectra of the photoanodes co-sensitized by **IBT3** with **IBT1** and **IBT2** are shown in Fig. S20 (ESI†). Compared with the photoanodes without co-sensitization, the absorption spectra of the two new photoanodes show significant differences in the range of 400–500 nm, and the valleys of **IBT1** and **IBT2** are filled up by an absorption peak that appears for **IBT3** in the same region. Thus, we utilize **IBT3** as a co-sensitizer to make up the weak absorption between 300 and 500 nm of **IBT1** and **IBT2**. The corresponding photovoltaic parameters are listed in Table 3 and Fig. 5. For the devices co-sensitized by **IBT3** with **IBT1** and **IBT2**, the PCEs increase to 7.85% and 7.64%, respectively, which reach that of the reference dye **N719** (7.85%) under the same conditions. After co-sensitization, the loading amount of each dye was measured (Table 3). The results manifest that using a co-sensitizer can minimize the loss of low loading amount resulting from a bulky anti-aggregation π-bridge and improve the available photovoltaic performance.

3.8 Electrochemical impedance spectroscopy

The charge recombination rate of a device has an important influence on V_{oc}. At the same photocarrier generation flux, the charge recombination is primarily determined by the interfacial electron recombination rate based on the surface of TiO_2. To study the charge recombination dynamics, electrochemical impedance spectra (EIS) of DSSCs were obtained under 0.68 V bias voltage in the dark. The results are shown in Fig. 6 and the relevant parameters are listed in Table 4. The small semicircle represents the charge transfer resistance (R_{ce}) at the interface of the counter electrode and electrolyte. The second semicircle represents the charge transfer resistance (R_{rec}) at the interface of TiO_2, dye and electrolyte. The R_{ce} values of the three dyes are similar, which may be due to the same batch of counter electrode and electrolyte. However, the radius of the large semicircle increased in the order: **IBT2** < **IBT3** < **IBT1**, which is in agreement with the variation of V_{oc}. The results also indicate that the circle alkyl chain can weaken charge recombination more effectively than the linear alkyl chain because a tight compact

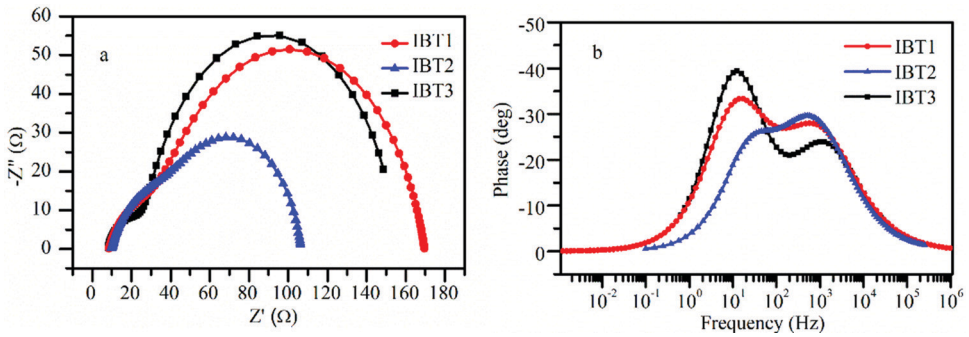

Fig. 6 Nyquist (a) and Bode phase plots (b) of electrochemical impedance spectra (EIS) for DSSCs based on **IBT1–3**.

Published on 26 July 2019. Downloaded on 1/29/2026 9:17:27 PM.

Table 4 Parameters of the electrochemical impedance spectra for DSSCs

Dye	R_{ce} (Ω cm^{-2})	R_{rec} (Ω cm^{-2})	CPE2 (μF)	τ (ms)
IBT1	27.34	133.7	460	61.5
IBT2	33.67	63.1	346	21.8
IBT3	19.21	128.1	396	50.7

layer is formed on the surface of TiO_2. A large steric hindrance is obtained by SPDF, but charge recombination is easier because the gap between the two molecular frames is oversized. This observation can also be verified in the Bode phase plots (Fig. 6b). The peaks with the frequency lying in the range of 10^{-1}–10^{2} Hz represent the electron transfer frequency at the interface of TiO_2/dye/electrolyte. Moreover, the electron lifetime (τ) can be calculated by $\tau_{ct} = R_{rec} \times C_{CPE}$.[74,75] The corresponding electron lifetime values of DSSCs based on **IBT1**, **IBT2** and **IBT3** are 61.5 ms, 21.8 ms and 50.7 ms, respectively. The shorter electron lifetime stands for a higher dark current.

The electrochemical impedance spectra (EIS) were also recorded under different applied voltages in the dark.[76,77] The results are shown in Fig. S21 (ESI†). At a fixed potential, the R_{rec} values increased in the order of **IBT2** < **IBT3** < **IBT1**, consistent with the variation of V_{oc}. This result indicates that the introduction of EIMW is beneficial to the suppression of charge recombination. After co-sensitization, the two new devices present higher R_{rec} values than the DSSCs without co-sensitization, respectively (Fig. S22, ESI†). This result is consistent with the variation of the V_{oc}.

4. Conclusion

Two novel D–A–π–A metal-free organic dyes **IBT1** and **IBT2** with EIMW and SPDF as anti-aggregation π-bridges were designed, synthesized and applied in DSSCs. Due to the excellent photoelectric performance of EIMW and SPDF, **IBT1** achieves a higher V_{oc} and **IBT2** shows a wider IPCE response, respectively. In addition, the co-adsorption experiment with CDCA demonstrates that EIMW and SPDF as π-bridges inhibit dye aggregation more significantly than DHBT. After dyes **IBT1** and **IBT2** are co-sensitized with **IBT3**, the new devices exhibit the same high efficiencies as that of **N719**. This work not only provides an anti-aggregation strategy by structural engineering of the π-spacer, but also two novel dyes as promising candidates for efficient DSSCs.

Conflicts of interest

The authors declare no competing financial interest.

Acknowledgements

We are grateful to the National Natural Science Foundation of China (21572069, 21772045), the National Key Research and Development Program of China (2016YFA0602900), and the Natural Science Foundation of Guangdong Province, China (2018B030311008).

References

1 A. Hagfeldt, G. Boschloo, L. Sun, L. Kloo and H. Pettersson, *Chem. Rev.*, 2010, **110**, 6595–6663.
2 L. L. Li and E. W. Diau, *Chem. Soc. Rev.*, 2013, **42**, 291–304.
3 J. Gong, K. Sumathy, Q. Qiao and Z. Zhou, *Renewable Sustainable Energy Rev.*, 2017, **68**, 234–246.
4 H. Meier, Z.-S. Huang and D. Cao, *J. Mater. Chem. C*, 2017, **5**, 9828–9837.
5 A. Mishra, M. K. R. Fischer and P. Bäuerle, *Angew. Chem., Int. Ed.*, 2009, **48**, 2474–2499.
6 M. Freitag, J. Teuscher, Y. Saygili, X. Zhang, F. Giordano, P. Liska, J. Hua, S. M. Zakeeruddin, J.-E. Moser, M. Grätzel and A. Hagfeldt, *Nat. Photonics*, 2017, **11**, 372–378.
7 X. Li, X. Zhang, J. Hua and H. Tian, *Mol. Syst. Des. Eng.*, 2017, **2**, 98–122.
8 S. Chaurasia, C.-J. Liang, Y.-S. Yen and J. T. Lin, *J. Mater. Chem. C*, 2015, **3**, 9765–9780.
9 B. O'Regan and M. Grätzel, *Nature*, 1991, **353**, 737.
10 C. Li, L. Luo, D. Wu, R. Jiang, J. Lan, R. Wang, L. Huang, S. Yang and J. You, *J. Mater. Chem. A*, 2016, **4**, 11829–11834.
11 Y. Huang, W.-C. Chen, R. Ghadari, X.-P. Liu, X.-Q. Fang, T. Yu and F.-T. Kong, *J. Power Sources*, 2018, **396**, 559–565.
12 G. Saritha, R. V. Mangalaraja and S. Anandan, *Sol. Energy*, 2017, **146**, 150–160.
13 J. S. Ni, W. S. Kao, H. J. Chou and J. T. Lin, *ChemSusChem*, 2015, **8**, 2932–2939.
14 Z.-S. Huang, H. Meier and D. Cao, *J. Mater. Chem. C*, 2016, **4**, 2404–2426.
15 J. H. Yum, E. Baranoff, F. Kessler, T. Moehl, S. Ahmad, T. Bessho, A. Marchioro, E. Ghadiri, J. E. Moser, C. Yi, M. K. Nazeeruddin and M. Gratzel, *Nat. Commun.*, 2012, **3**, 631.
16 G. Wu, F. Kong, Y. Zhang, X. Zhang, J. Li, W. Chen, W. Liu, Y. Ding, C. Zhang, B. Zhang, J. Yao and S. Dai, *J. Phys. Chem. C*, 2014, **118**, 8756–8765.
17 P. Dai, L. Yang, M. Liang, H. Dong, P. Wang, C. Zhang, Z. Sun and S. Xue, *ACS Appl. Mater. Interfaces*, 2015, **7**, 22436–22447.
18 L. Zhang, X. Yang, W. Wang, G. G. Gurzadyan, J. Li, X. Li, J. An, Z. Yu, H. Wang, B. Cai, A. Hagfeldt and L. Sun, *ACS Energy Lett.*, 2019, **4**, 943–951.
19 X. Xie, D. Sun, Y. Wei, Y. Yuan, J. Zhang, Y. Ren and P. Wang, *J. Mater. Chem. A*, 2019, **7**, 11338–11346.
20 K. Kakiage, Y. Aoyama, T. Yano, K. Oya, J. Fujisawa and M. Hanaya, *Chem. Commun.*, 2015, **51**, 15894–15897.
21 Z. Ning and H. Tian, *Chem. Commun.*, 2009, 5483–5495.
22 X. Ren, S. Jiang, M. Cha, G. Zhou and Z.-S. Wang, *Chem. Mater.*, 2012, **24**, 3493–3499.
23 C.-Y. Lo, D. Kumar, S.-H. Chou, C.-H. Chen, C.-H. Tsai, S.-H. Liu, P.-T. Chou and K.-T. Wong, *ACS Appl. Mater. Interfaces*, 2016, **8**, 27832–27842.
24 H.-H. Gao, X. Qian, W.-Y. Chang, S.-S. Wang, Y.-Z. Zhu and J.-Y. Zheng, *J. Power Sources*, 2016, **307**, 866–874.
25 G. S. Selopal, H.-P. Wu, J. Lu, Y.-C. Chang, M. Wang, A. Vomiero, I. Concina and E. W.-G. Diau, *Sci. Rep.*, 2016, **6**, 18756.

 This journal is © The Royal Society of Chemistry 2019

Published on 26 July 2019. Downloaded on 1/29/2026 9:17:27 PM.

26 D. Joly, M. Godfroy, L. Pellejà, Y. Kervella, P. Maldivi, S. Narbey, F. Oswald, E. Palomares and R. Demadrille, *J. Mater. Chem. A*, 2017, **5**, 6122–6130.
27 Y. K. Eom, S. H. Kang, I. T. Choi, Y. Yoo, J. Kim and H. K. Kim, *J. Mater. Chem. A*, 2017, **5**, 2297–2308.
28 F. Lu, G. Yang, Q. Xu, J. Zhang, B. Zhang and Y. Feng, *Dyes Pigm.*, 2018, **158**, 195–203.
29 J. S. Ni, Y. C. Yen and J. T. Lin, *Chem. Commun.*, 2015, **51**, 17080–17083.
30 L.-W. Ma, Z.-S. Huang, S. Wang, H. Meier and D. Cao, *Dyes Pigm.*, 2017, **145**, 126–135.
31 X. Lu, Q. Feng, T. Lan, G. Zhou and Z.-S. Wang, *Chem. Mater.*, 2012, **24**, 3179–3187.
32 J. Yang, P. Ganesan, J. Teuscher, T. Moehl, Y. J. Kim, C. Yi, P. Comte, K. Pei, T. W. Holcombe, M. K. Nazeeruddin, J. Hua, S. M. Zakeeruddin, H. Tian and M. Grätzel, *J. Am. Chem. Soc.*, 2014, **136**, 5722–5730.
33 G. Wang, Z. Liu, Y. Deng, L. Xie and S. Tan, *Dyes Pigm.*, 2017, **145**, 427–435.
34 Y. Hao, Y. Saygili, J. Cong, A. Eriksson, W. Yang, J. Zhang, E. Polanski, K. Nonomura, S. M. Zakeeruddin, M. Grätzel, A. Hagfeldt and G. Boschloo, *ACS Appl. Mater. Interfaces*, 2016, **8**, 32797–32804.
35 C. Aumaitre, C. Rodriguez-Seco, J. Jover, O. Bardagot, F. Caffy, Y. Kervella, N. López, E. Palomares and R. Demadrille, *J. Mater. Chem. A*, 2018, **6**, 10074–10084.
36 M. Mao, X.-L. Zhang, X.-Q. Fang, G.-H. Wu, Y. Ding, X.-L. Liu, S.-Y. Dai and Q.-H. Song, *Org. Electron.*, 2014, **15**, 2079–2090.
37 J.-B. Wang, X.-Q. Fang, X. Pan, S.-Y. Dai and Q.-H. Song, *Chem. – Asian J.*, 2012, **7**, 696–700.
38 S. Nagane, A. Ichake, I. Agrawal, A. Sadhanala, R. H. Friend, S. Ogale and P. P. Wadgaonkar, *ChemPlusChem*, 2017, **82**, 280–286.
39 S. Qu, C. Qin, A. Islam, Y. Wu, W. Zhu, J. Hua, H. Tian and L. Han, *Chem. Commun.*, 2012, **48**, 6972.
40 Y. Wu, X. Zhang, W. Li, Z.-S. Wang, H. Tian and W. Zhu, *Adv. Energy Mater.*, 2012, **2**, 149–156.
41 Z. Chai, M. Wu, M. Fang, S. Wan, T. Xu, R. Tang, Y. Xie, A. Mei, H. Han, Q. Li and Z. Li, *Adv. Energy Mater.*, 2015, **5**, 1500846.
42 J. Luo, X. Wang, L. Fan, G. Li, Q. Qi, K.-W. Huang, T. L. Dexter Tam, J. Zhang, Q. Wang and J. Wu, *J. Mater. Chem. C*, 2016, **4**, 3709–3714.
43 Q. Chai, W. Li, Y. Wu, K. Pei, J. Liu, Z. Geng, H. Tian and W. Zhu, *ACS Appl. Mater. Interfaces*, 2014, **6**, 14621–14630.
44 K. Chaitanya, B. M. Heron and X.-H. Ju, *Dyes Pigm.*, 2017, **141**, 501–511.
45 W. Zhang, Y. Wu, X. Li, E. Li, X. Song, H. Jiang, C. Shen, H. Zhang, H. Tian and W.-H. Zhu, *Chem. Sci.*, 2017, **8**, 2115–2124.
46 X. Li, B. Xu, P. Liu, Y. Hu, L. Kloo, J. Hua, L. Sun and H. Tian, *J. Mater. Chem. A*, 2017, **5**, 3157–3166.
47 X. Li, Y. Hu, I. Sanchez-Molina, Y. Zhou, F. Yu, S. A. Haque, W. Wu, J. Hua, H. Tian and N. Robertson, *J. Mater. Chem. A*, 2015, **3**, 21733–21743.
48 X. Wang, J. Yang, H. Yu, F. Li, L. Fan, W. Sun, Y. Liu, Z. Y. Koh, J. Pan, W.-L. Yim, L. Yan and Q. Wang, *Chem. Commun.*, 2014, **50**, 3965–3968.
49 M. Xu, X. Hu, Y. Zhang, X. Bao, A. Pang and J.-K. Fang, *ACS Appl. Energy Mater.*, 2018, **1**, 2200–2207.
50 R. Milan, G. S. Selopal, M. Cavazzini, S. Orlandi, R. Boaretto, S. Caramori, I. Concina and G. Pozzi, *Sci. Rep.*, 2017, **7**, 15675.
51 E. Colom, J. M. Andrés-Castán, D. Barrios, I. Duerto, S. Franco, J. Garín, J. Orduna, B. Villacampa and M. J. Blesa, *Dyes Pigm.*, 2019, **164**, 43–53.
52 J. Liu, Y. Numata, C. Qin, A. Islam, X. Yang and L. Han, *Chem. Commun.*, 2013, **49**, 7587.
53 K. Zeng, Y. Lu, W. Tang, S. Zhao, Q. Liu, W. Zhu, H. Tian and Y. Xie, *Chem. Sci.*, 2019, **10**, 2186–2192.
54 T. Hua, Z.-S. Huang, K. Cai, L. Wang, H. Tang, H. Meier and D. Cao, *Electrochim. Acta*, 2019, **302**, 225–233.
55 Y. Tang, Y. Wang, X. Li, H. Agren, W. H. Zhu and Y. Xie, *ACS Appl. Mater. Interfaces*, 2015, **7**, 27976–27985.
56 R. Bisht, S. Singh, K. Krishnamoorthy and J. Nithyanandhan, *J. Org. Chem.*, 2017, **82**, 1920–1930.
57 H. Dong, M. Liang, C. Zhang, Y. Wu, Z. Sun and S. Xue, *J. Phys. Chem. C*, 2016, **120**, 22822–22830.
58 W. Zhang, Y. Wu, H. Zhu, Q. Chai, J. Liu, H. Li, X. Song and W.-H. Zhu, *ACS Appl. Mater. Interfaces*, 2015, **7**, 26802–26810.
59 C. Chen, J.-Y. Liao, Z. Chi, B. Xu, X. Zhang, D.-B. Kuang, Y. Zhang, S. Liu and J. Xu, *J. Mater. Chem.*, 2012, **22**, 8994.
60 Z.-S. Huang, H.-L. Feng, X.-F. Zang, Z. Iqbal, H. Zeng, D.-B. Kuang, L. Wang, H. Meier and D. Cao, *J. Mater. Chem. A*, 2014, **2**, 15365–15376.
61 Z. Iqbal, W.-Q. Wu, H. Zhang, L. Han, X. Fang, L. Wang, D.-B. Kuang, H. Meier and D. Cao, *Org. Electron.*, 2013, **14**, 2662–2672.
62 K. Sugiyasu, Y. Honsho, R. M. Harrison, A. Sato, T. Yasuda, S. Seki and M. Takeuchi, *J. Am. Chem. Soc.*, 2010, **132**, 14754–14756.
63 H. Naoto, N. Takashi, M. Takuya, N. Hiroki, M. Keiko, M. Mikio and H. Hiroyuki, *Bull. Chem. Soc. Jpn.*, 2007, **80**, 371–386.
64 C. Zhao, T. Sakurai, S. Yoneda, S. Seki, M. Sugimoto, C. Oki, M. Takeuchi and K. Sugiyasu, *Chem. – Asian J.*, 2016, **11**, 2284–2290.
65 H. Hanamura and N. Nemoto, *Polymer*, 2014, **55**, 6672–6679.
66 Y. Wu, M. Marszalek, S. M. Zakeeruddin, Q. Zhang, H. Tian, M. Grätzel and W. Zhu, *Energy Environ. Sci.*, 2012, **5**, 8261.
67 S. Cai, X. Hu, Z. Zhang, J. Su, X. Li, A. Islam, L. Han and H. Tian, *J. Mater. Chem. A*, 2013, **1**, 4763.
68 J. He, W. Wu, J. Hua, Y. Jiang, S. Qu, J. Li, Y. Long and H. Tian, *J. Mater. Chem.*, 2011, **21**, 6054.
69 H.-L. Jia, Y.-C. Chen, L. Ji, L.-X. Lin, M.-Y. Guan and Y. Yang, *Dyes Pigm.*, 2019, **163**, 589–593.
70 D. Heredia, J. Natera, M. Gervaldo, L. Otero, F. Fungo, C. Y. Lin and K. T. Wong, *Org. Lett.*, 2010, **12**, 12–15.
71 G. Pozzi, S. Orlandi, M. Cavazzini, D. Minudri, L. Macor, L. Otero and F. Fungo, *Org. Lett.*, 2013, **15**, 4642–4645.

72 C. H. Huang and Y. J. Chang, *Tetrahedron Lett.*, 2014, **55**, 4938–4942.
73 H. Chen, G. Lyu, Y. Yue, T. Wang, D.-P. Li, H. Shi, J. Xing, J. Shao, R. Zhang and J. Liu, *J. Mater. Chem. C*, 2019, **7**, 7249–7258.
74 Z. Shen, J. Chen, X. Li, X. Li, Y. Zhou, Y. Yu, H. Ding, J. Li, L. Zhu and J. Hua, *ACS Sustainable Chem. Eng.*, 2016, **4**, 3518–3525.
75 J.-H. Park, D. G. Nam, B.-M. Kim, M. Y. Jin, D.-H. Roh, H. S. Jung, D. H. Ryu and T.-H. Kwon, *ACS Energy Lett.*, 2017, **2**, 1810–1817.
76 K. T. Dembele, G. S. Selopal, C. Soldano, R. Nechache, J. C. Rimada, I. Concina, G. Sberveglieri, F. Rosei and A. Vomiero, *J. Phys. Chem. C*, 2013, **117**, 14510–14517.
77 H. Li, M. Fang, R. Tang, Y. Hou, Q. Liao, A. Mei, H. Han, Q. Li and Z. Li, *J. Mater. Chem. A*, 2016, **4**, 16403–16409.

Published on 26 July 2019. Downloaded on 1/29/2026 9:17:27 PM.

This journal is © The Royal Society of Chemistry 2019